Biosensors and Bioelectronics 135 (2019) 88–94

Contents lists available at ScienceDirect

Biosensors and Bioelectronics

journal homepage: www.elsevier.com/locate/bios

Fabrication of hierarchical MIL-68(In)-NH_2/MWCNT/CdS composites for constructing label-free photoelectrochemical tetracycline aptasensor platform

Xue Zhang[a], Tao Yan[a,*], Tingting Wu[a], Yixuan Feng[a], Meng Sun[a], Liangguo Yan[a], Bin Du[a], Qin Wei[b]

[a] School of Water Conservancy and Environment, University of Jinan, Jinan, 250022, PR China
[b] Key Laboratory of Interfacial Reaction & Sensing Analysis in Universities of Shandong, School of Chemistry and Chemical Engineering, University of Jinan, Jinan, 250022, China

ARTICLE INFO

Keywords:
Label-free
PEC aptasensor
MIL-68(In)-NH_2/MWCNT/CdS
Tetracycline
Metal-organic frameworks

ABSTRACT

It is essential to develop a highly efficient detection platform for tetracycline (Tc). Herein, based on well-designed hierarchical MIL-68(In)-NH_2/MWCNT/CdS composites as a highly efficient transducer, a label-free visible light driven photoelectrochemical (PEC) aptasensor was systematically fabricated. Characterization results indicate that the forming of MIL-68(In)-NH_2/CdS heterojunction remarkable facilitated the transfer and inhibited the recombination of charge carriers. Moreover, the transfer properties of multiwalled carbon nanotubes (MWCNTs) further improved the photoelectric conversion efficiency by adjusting electron transport routes. The aptamer as a biorecognition unit was grafted on the modified electrode by chemical bonding effect, and Tc molecules could be captured through the specific interaction of aptamer and Tc in solution. The concentration of Tc was detected by observing the fluctuation of photocurrent signals. Under optimized conditions, the proposed aptasensor showed the broad linear range from 0.1 nmol L^{-1} to 1 μmol L^{-1} with a low detection limit (LOD) of 0.015 nmol L^{-1}. Furthermore, the high sensitivity, excellent reproducibility and favorable stability of the PEC sensing platform indicated the potential applications for antibiotic residues detecting in environmental media.

1. Introduction

Tetracycline (Tc), a sort of broad-spectrum antibiotic, possess distinct bacteriostatic activity against both Gram-positive and Gram-negative (Han et al., 2018). Due to their inexpensive and effectiveness, it has been extensively used in the prophylaxis and therapy of human and animal infections, and also in animal husbandry as growth promoters (Choi et al., 2007). Most importantly, due to the disorderly abuse of Tc, it has caused long-term environmental residues *via* ecological cycle (Liu et al., 2013; Song et al., 2018), and followed by the imperceptible accompanying derivatization of stubborn resistance genes (Yu et al., 2018), which may cause more serious ecological high-potential risks. Currently, various methods have been developed for Tc detection, including high performance liquid chromatography (HPLC) (Liu et al., 2017), colorimetric analysis (Wang et al., 2016b), fluorescence (Zhou et al., 2018), chemiluminescence (Zhu et al., 2016) and electrochemical immunoassays (Devkota et al., 2018) et al. However, the methods mentioned above usually have the drawbacks of complicated operation and expensive equipment. Therefore, it is essential to exploit a rapid, simple, low-cost and specific method for high-efficiency Tc detection.

Photoelectrochemical (PEC) sensor has attracted widespread attention as a wonderful analytical technique for biomedical molecules and environmental pollutants detection due to its high sensitivity (Wang et al., 2018b), low cost (Zhang et al., 2016) and low background noise (Zang et al., 2017). For PEC sensors, the well-designed photoactive electrode is core component, which played a key role in the conversion of photonic energy to electrochemical detectable signal. Numerous excellent photochemical active materials have been developed for the fabrication of PEC photoactive electrode, including metal oxides (Dai et al., 2014), metal chalcogenides (Wang et al., 2017), diversified quantum dots (Chen et al., 2018), novel carbon-based functional materials (Wu et al., 2018b) and so on, which accelerated the technological innovation of PEC sensor in testing application. However, the electron transfer tardiness and highly recombination of carriers are always knotty problems to deal with. Consequently, it is still to be expected to explore photoactive matrix with excellent activity and

* Corresponding author.
E-mail address: yantujn@163.com (T. Yan).

https://doi.org/10.1016/j.bios.2019.03.062
Received 2 February 2019; Received in revised form 27 March 2019; Accepted 29 March 2019
Available online 04 April 2019
0956-5663/

stability, which is an urgent research task.

Metal-organic frameworks (MOFs), a kind of inorganic-organic hybrid material (Sanchez et al., 2005), has been given much attention considering their multitudinous applications (Liu and Li, 2016; Ma et al., 2016; Qin et al., 2012). Since García and his co-workers researched on the semiconductor properties and photoactivity of MOF-5 and Zr-benzenecarboxylate MOFs (Alvaro et al., 2007; Dhakshinamoorthy et al., 2010; Gomes Silva et al., 2010), the photoactive MOFs material has become one of research hot spots to solve the energy shortage and environmental protection issue (Bagheri et al., 2017; Leng et al., 2018; Li et al., 2018; Liao et al., 2018; Wang et al., 2015). Recently, Our group has interests in the synthesis of MOFs to improve their photoactivity and stability for environmental sensing applications (Wu et al., 2018a). MIL-68(In)-NH_2 is an amine functionalized indium-based MOFs material consisting of transition metal-oxo clusters and organic-ligands (Wu et al., 2012), which now receiving extensive attention, due to its high thermal stability, adjustability and photo-responsiveness. Recently, Wu's group has firstly discussed the performance of MIL-68(In)-NH_2 on the reduction of Cr(VI) under visible light irradiation (Liang et al., 2015). Afterwards, Xiao's group has reported that the coupling of MWCNTs and MIL-68(In)-NH_2 could effectively improve the photogenerated charge separation and accelerate the reduction of Cr(VI) under visible light (Pi et al., 2017). Besides, Cheng's group has synthesized MIL-68(In)-NH_2/GrO composites that the photodegradation activity for amoxicillin significantly improved comparing with pure MIL-68(In)-NH_2 (Yang et al., 2017). As mentioned above, multiple studies about MIL-68(In)-NH_2 have testified its excellent photoactivity, which boosting its studies in environmental remediation. However, as far as we know, MIL-68(In)-NH_2 has not been explored in the field of PEC sensing. Inspired by these, novel MIL-68(In)-NH_2/MWCNT/CdS composites were developed in this context, and served as basis in sensing strategy for constructing PEC aptasensor.

Therefore, a label-free PEC sensing detection platform was fabricated basing on the hierarchical MIL-68(In)-NH_2/MWCNT/CdS nanostructure for the first time. The constructing process of MIL-68(In)-NH_2/MWCNT/CdS composites was described systematically. Firstly, MIL-68(In)-NH_2/MWCNT composites were prepared through solvothermal method, after which CdS nanoparticles (NPs) were *in-situ* deposited on the surface of MIL-68(In)-NH_2/MWCNT composites *via* hydrothermal method (Scheme 1A). The structures, morphologies, electrical and optical properties, and PEC performances of the as-prepared materials were investigated in details. The transfer properties of MWCNTs as well as the excellent visible-light absorption capacity of MIL-68(In)-NH_2/CdS heterojunction greatly improved the PEC performance. The modified electrode exhibits the highest photocurrent intensity at +0.5 V (vs. SCE) (saturated calomel electrode). In detecting process, the tetracycline-binding aptamer would specifically capture Tc molecules in solution, resulting to a raised photocurrent signal *via* the instantaneous reaction between trapped Tc molecules and photo-generated holes. The fabricated aptasensor exhibited good selectivity, high sensitivity, rapid response and wide linear range, indicating a broad application prospect for antibiotic residues detecting in environment.

2. Materials and methods

2.1. Materials and reagents

Indium nitrate hydrate ($In(NO_3)_3{\cdot}xH_2O$) and 2-aminoterephthalicacid (H_2ATA) were purchased from Shanghai Macklin Biochemical Co., Ltd. Tc aptamer with the following sequences: 5′-NH_2-$(CH_2)_6$-CGT ACG GAA TTC GCT AGC CCC CCG GCA GGC CAC GGC TTGGGT TGG TCC CAC TGC GCG TGG ATC CGA GCT CCA CGT G-3′ was obtained from Sangon Biotech Co., Ltd. N-hydroxysuccinimide (NHS) and 1-ethyl-3-(3-dimethylaminopropyl) carbodiimide hydrochloride (EDC) were obtained from Shanghai Aladdin Reagent Database Inc. The remaining details are shown in the supporting **materials.**

2.2. Apparatus

Energy dispersive spectrometer (EDS) images were obtained through field emission scanning electron microscope (SEM) (Zeiss, Germany). X-ray power diffraction (XRD) was obtained using a D8 advance X-ray diffractometer (Bruker AXS, Germany) with Cu K_α radiation (λ = 1.5406 A) at 40 kV and 40 mA. Electrochemical impedance spectroscopy (EIS) analysis was performed through an electrochemical workstation (Zahner Zennium PP211, Germany) with a three-electrode system in a 2.5 mmol L^{-1} $[Fe(CN)_6]^{3-/4-}$ solution containing 0.1 mol L^{-1} KCl. The frequency range was 0.1–10^5 Hz with amplitude of 5 mV. A three-electrode system was used throughout the measurements, composed of a Pt wire electrode as counter electrode, an Hg/

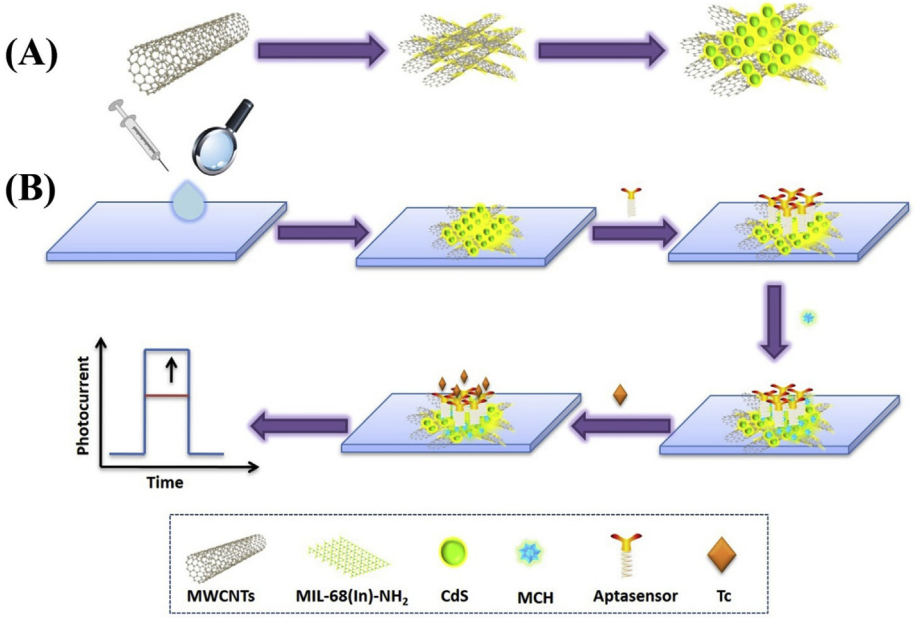

Scheme 1. The synthesis of MIL-68(In)-NH_2/MWCNT/CdS composites (A); the fabrication process of a PEC aptasensor for detection of Tc (B).

Hg_2Cl_2 electrode (SCE) as reference electrode and modified Indium-tin oxide (ITO) electrode as the working electrode. The remaining details are shown in the supporting **materials**.

2.3. Synthesis of MIL-68(In)-NH_2/MWCNT composites

Carboxyl-modified MWCNTs (MWCNT-COOH) were refined from raw MWCNTs according to the reported literature with slight modification (Wang et al., 2016a).

The MIL-68(In)-NH_2/MWCNT composites were synthesized by a dynamic solvothermal method (Pi et al., 2017), and the MIL-68(In)-NH_2 powder was fabricated through a similar procedure in the absence of MWCNT. The remaining details are shown in the supporting **materials**.

2.4. Synthesis of MIL-68(In)-NH_2/MWCNT/CdS composites

For MIL-68(In)-NH_2/MWCNT/CdS composites, the *in-situ* deposition strategy was conducted according to the literature (He et al., 2013; Ke et al., 2015). The remaining details are shown in the supporting **materials**.

2.5. Fabrication of the PEC aptasensor

Before preparing the aptasensor, indium-tin-oxide (ITO) substrates were cut into 1.8 × 0.8 cm^2 pieces and were ultrasonically washed with acetone, ethanol, and ultrapure water for 30 min, and lastly dried by nitrogen for use.

Scheme 1B exhibited the fabrication process of the PEC aptasensor. Firstly, 9 μL MIL-68(In)-NH_2/MWCNT/CdS solution was dropped onto an ITO electrode and dried under the infrared lamp for 30 min. After drying, 3 μL of EDC/NHS (containing 0.01 mol L^{-1} of EDC and 0.002 mol L^{-1} of NHS) was dropped onto the ITO/MIL-68(In)-NH_2/MWCNT/CdS electrode and cultivated for 30 min to activate the −COOH groups then rinsing with washing buffer. Whereafter, 5 μL aptamer (dispersed in 0.01 mol L^{-1} PBS) was immobilized onto the electrode and incubated at 4 °C for 1 h, then washed with PBS (0.01 mol L^{-1}) to wash down physically absorbed aptamer. After rinsing with PBS, 5 μL mercaptoethanol (MCH) (1 mmol L^{-1}) solution was incubated on the ITO/MIL-68(In)-NH_2/MWCNT/CdS/aptamer electrodes for 1 h to block non-specific sites, followed by washing. Finally, 5 μL Tc solutions with different concentration was dropped on the modified electrode surface and incubated at 4 °C for 1 h and rinsed slightly with PBS buffer.

2.6. PEC detection of Tc

Tc detection was carried out by an electrochemical workstation (CHI 760E Chenhua Instrument Company, Shanghai, China). The photocurrent was measured with a three-electrode system using a 300 W xenon lamp (λ > 420 nm) as light source, and the applied potential was +0.5 V (vs. SCE). The buffer solution was PBS (pH = 7.4) that prepared from $Na_2HPO_4{\cdot}12H_2O$ (0.1 mol L^{-1}) and KH_2PO_4 (0.1 mol L^{-1}). 10 mL electrolytes were used for testing, and the distance between the light source and the electrode was about 15 cm.

3. Results and discussions

3.1. Characterization of the synthesized materials

The morphological of as-prepared materials are characterized by SEM and TEM. As shown in Fig. 1A, MIL-68(In)-NH_2 exhibits an aggregation of two-dimensional (2D) nanosheets, which is the consequent of continual accumulating of MIL-68(In)-NH_2 nanocrystals during the synthetic process. For the MIL-68(In)-NH_2/MWCNT composites, it could be found that the MIL-68(In)-NH_2 still kept the nanosheets feature and tendency to grow along the functionalized MWCNTs (Fig. 1B), which is similar to the literature reports (Pi et al., 2017). As shown in Fig. 1C, the pure CdS aggregates together to form nanospheres with a loose structure. However, the morphology is quite different from that of pure CdS, when an appropriate amount of MIL-68(In)-NH_2/MWCNT was added during the synthesis of MIL-68(In)-NH_2/MWCNT/CdS composites. As shown in Fig. 1D, the CdS NPs possess much smaller average size than pure CdS nanospheres, and well dispersed on the surface of MIL-68(In)-NH_2/MWCNT composites. It can be deduced that the MIL-68(In)-NH_2/MWCNT serves as a support can effectively inhibit the growth and aggregation of CdS NPs. This result is consistent with literature reports (Ke et al., 2015). The excellent distribution of CdS NPs on the surface of MIL-68(In)-NH_2/MWCNT guarantees effective PEC properties of MIL-68(In)-NH_2/MWCNT/CdS composites. The HRTEM image (Fig. 1 E) showed the clear lattice fringes of d = 0.29 nm corresponding to (111) plan of CdS, as well as the intimate vague fringes of adjacent component. This intimate contact enables the formation of a high-efficiency heterojunction between MIL-68(In)-NH_2 and CdS, which is conducive to transfer and separation of charge carriers. Besides, the functionalized MWCNTs interspersed therein further promoting the rapid transfer of photoelectrons by adjusting electron transport routes. Meanwhile, the EDS analysis (Fig. 1F) and elemental mapping images (EMIs) (Fig. S1) revealed the existence of C, O, N, Cd, S and In elements.

The XRD patterns of MIL-68(In)-NH_2, MIL-68(In)-NH_2/MWCNT, and MIL-68(In)-NH_2/MWCNT/CdS were shown in Fig. 2A and B, the pattern of MIL-68(In)-NH_2 was well agreement with those reported previously (curve a) (Liang et al., 2015; Pi et al., 2017; Yang et al., 2017). A weak diffraction peak occurred at 26.2° matching well with (002) plane of the MWCNTs (Sun et al., 2014), and the lower diffraction peaks (curve b) caused by the low dosage of MWCNTs. Besides, as for MIL-68(In)-NH_2/MWCNT/CdS composites (curve c), new diffraction peaks appearing at 26.5°, 43.9° and 52.1° were clearly observed, which could be assigned to (111), (220) and (311) diffraction planes of CdS (JCPDS No. 10–0454), indicating the MIL-68(In)-NH_2/MWCNT/CdS composites were successfully synthesized.

XPS is an effective way to investigate and characterize the chemical composition of MIL-68(In)-NH_2/MWCNT/CdS composites. As presented in Fig. 2C, the elements of C, N, O, In, Cd and S appeared in the survey spectrum. The detailed XPS spectrum analyses are shown in the Supporting **information** (Fig. S2).

3.2. Mechanism exploration

The UV-vis diffuse-reflectance spectra of MIL-68(In)-NH_2, MIL-68(In)-NH_2/MWCNT, and MIL-68(In)-NH_2/MWCNT/CdS were displayed in Fig. S3A. It could be observed that the absorption edge of MIL-68(In)-NH_2 was located at 480 nm, which matched well with its indirect band-gap energy of 2.79 eV, proving the efficient absorption and utilization of visible light. The absorption edge of MIL-68(In)-NH_2/MWCNT and MIL-68(In)-NH_2/MWCNT/CdS were estimated at 525 nm and 625 nm, respectively, which showed a red-shift after the introduction of MWCNTs and CdS, indicating their band-gap narrowing, which is favorable for utilizing solar light efficiently.

To further characterize the flat band potentials (E_{fb}) as well as the valence band potentials (E_{VB}) and conduction band potentials (E_{CB}) of the as-prepared samples, the Mott-Schottky (M-S) plot was performed. The positive slope of M-S plot in Fig. S3B demonstrates n-type behavior of MIL-68(In)-NH_2 (Spagnol et al., 2009), and the E_{fb} was obtained by extrapolating the M-S plot to $1/C^2 = 0$ (Swain et al., 2017). Hence, the E_{fb} of MIL-68(In)-NH_2 was probably about −0.78 V (vs. SCE), corresponding to a potential of −0.54 V (vs. NHE). It has been reported that the E_{fb} of n-type semiconductors are more negative than the E_{CB} (approximately 0.1–0.2 V) (Li et al., 2010). Thereby, the E_{CB} and E_{VB} of MIL-68(In)-NH_2 were calculated to be −0.64 V and +2.15 V, respectively. It is very close to the values reported in the literature (Yang et al., 2017). Besides, the E_{CB} and E_{VB} of CdS could be obtained from the

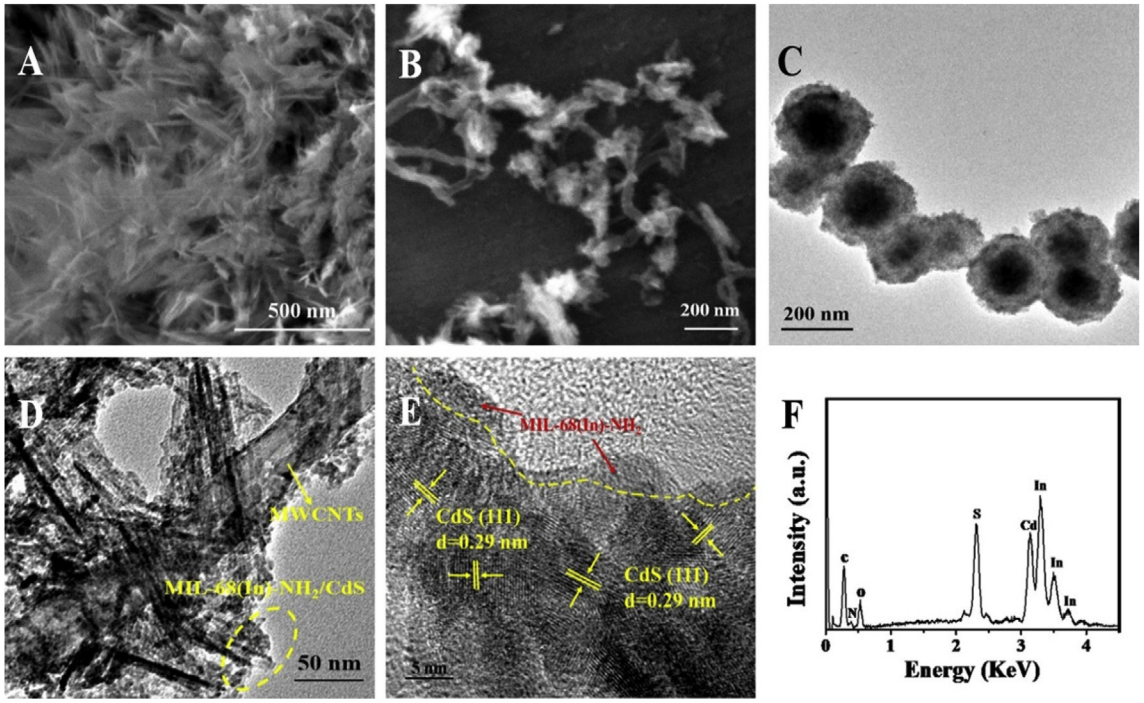

Fig. 1. SEM images of MIL-68(In)-NH_2 (A), MIL-68(In)-NH_2/MWCNT (B), TEM images of CdS (C), MIL-68(In)-NH_2/MWCNT/CdS (D), HRTEM image of. MIL-68(In)-NH_2/MWCNT/CdS (E); EDS spectrum of MIL-68(In)-NH_2/MWCNT/CdS (F).

literature (Yu et al., 2014).

Photoluminescence (PL) measurements were employed to further study the electron-transfer process of the as-prepared samples (Cheng et al., 2014). When excited at 365 nm, MIL-68(In)-NH_2 showed a strong and broad emission peak at ~ 465 nm while the MIL-68(In)-NH_2/MWCNT diminished dramatically, which could be attributed to the incorporating of MWCNTs promoted the charge transfer. For the MIL-68(In)-NH_2/MWCNT/CdS composites, the peak is nearly nonluminous (Fig. S3C), this could be attributed to the forming of MIL-68(In)-NH_2/CdS heterojunction remarkable suppressed the radiative electron-hole recombination.

The charge-transfer mechanism and PEC performance was probed in this work. Concretely, as shown in Fig. 3A, under visible light irradiation, both MIL-68(In)-NH_2 and CdS could be excited, due to the well-matched overlapping energy band structure, the photogenerated electrons transferred from CdS to MIL-68(In)-NH_2, and then injected into the ITO, thus generating the photocurrent response. Meanwhile, the holes remained in MIL-68(In)-NH_2 would transfer to the VB of CdS and subsequently migrate to the liquid-solid interface. The E_{VB} of CdS was +1.7 V (vs. NHE), which could not oxidize OH^- (OH^-/·OH = +1.89 V vs. NHE) and H_2O (H_2O/·OH = +2.72 V vs. NHE) into ·OH (Tachikawa et al., 2007), consequently, the holes accumulated on the surface of electrode could directly oxidize Tc molecules. What's more, MWCNTs as a fast transmission channel can effective facilitate the rapid transfer of electrons to ITO. As a result, the recombination efficiency of photogenerated electrons and holes was reduced, and the photocurrent was significantly improved (Liu et al., 2009; Zhao et al., 2014).

In order to examine the PEC behavior of different electrodes, a comparative trial was investigated. EIS analysis using $[Fe(CN)_6]^{3-/4-}$ as redox probe, the equivalent circuit including the solution resistance (R_s), the Warburg impendence (Z_ω), the double layer capacitance (C_{dl}) and the apparent charge-transfer resistance (R_{et}). The ZSimpWin software simulated equivalent circuit and the fitted values were shown in Table S1. As shown in Fig. 3B, R_{et} value of ITO/MIL-68(In)-NH_2 (curve a) and ITO/MIL-68(In)-NH_2/MWCNT (curve b) was about 35.36 Ω and 32.04 Ω, respectively, implying MWCNTs could effectively enhance electron transport ability of the pristine MIL-68(In)-NH_2, which was consistent with the PEC test results (Fig. 3C curve a and b). The R_{et} of ITO/MIL-68(In)-NH_2/MWCNT/CdS (curve e, 13.7 Ω) was the smallest compared to ITO/CdS (curve c, 19.16 Ω) and ITO/MIL-68(In)-NH_2/CdS (curve d, 17.19 Ω), meanwhile, the photocurrent intensity of the ITO/

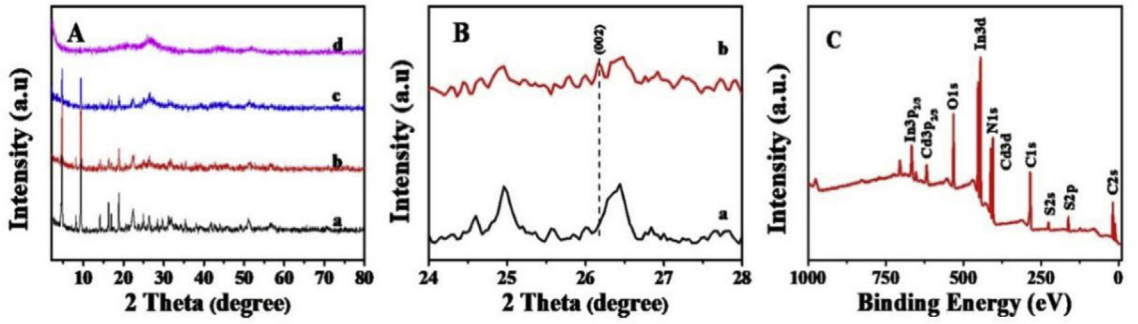

Fig. 2. XRD spectrum of (a) MIL-68(In)-NH_2, (b) MIL-68(In)-NH_2/MWCNT, (c) MIL-68(In)-NH_2/MWCNT/CdS and (d) CdS (A); XRD patterns of (a). MIL-68(In)-NH_2, (b) MIL-68(In)-NH_2/MWCNT (B); XPS patterns of MIL-68(In)-NH_2/MWCNT/CdS (C).

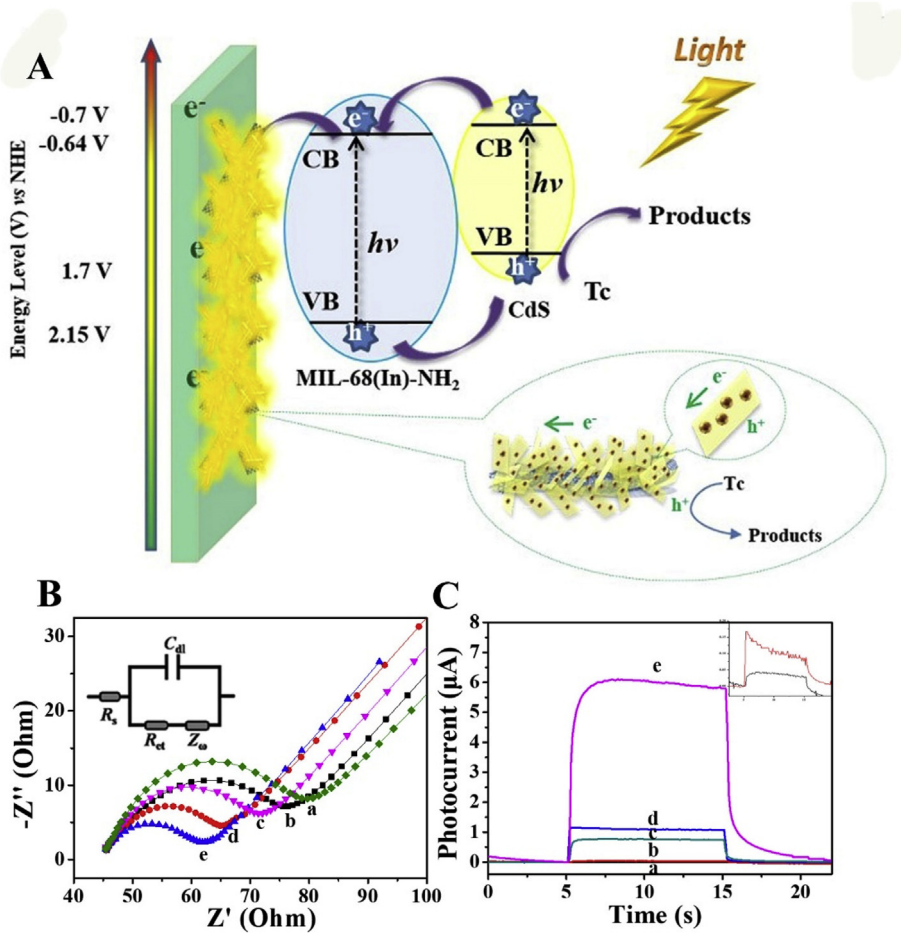

Fig. 3. (A) Schematic illustration of the photoelectrochemical aptasensor; (B) EIS spectra and (C) The transient photocurrent responses of: (a) MIL-68(In)-NH_2, (b) MIL-68(In)-NH_2/MWCNT, (c) CdS, (d) MIL-68(In)-NH_2/CdS and (e) MIL-68(In)-NH_2/MWCNT/CdS.

MIL-68(In)-NH_2/MWCNT/CdS (Fig. 3C curve e) was 7.8-fold and 5.5-fold enhancement compared to ITO/CdS and ITO/MIL-68(In)-NH_2/CdS (Fig. 3C curve c and d), indicating that the CdS/MIL-68(In)-NH_2 heterojunction can accelerate electron transfer to cause R_{et} value to decrease.

3.3. Characterization of the fabricated PEC aptasensor

EIS as a powerful tool was adopted to describe the transfer of electrons on the electrode interface. As demonstrated in Fig. 4A, the bare ITO exhibited a fairly small semicircle (curve a, R_{et} = 11.47), after the MIL-68(In)-NH_2/MWCNT/CdS was dropped onto the ITO, the diameter of the semicircle has increased (curve b, R_{et} = 13.7), indicating the successful modification of MIL-68(In)-NH_2/MWCNT/CdS on ITO electrode. Then, the R_{et} value drastically increased after aptamer was immobilized on the modified electrode (curve c, R_{et} = 26.22), which was attributed to the electrostatic repulsion between negatively charged phosphate backbone of the aptamer molecules and negatively charged redox species of the $[Fe(CN)6]^{3-/4-}$ (Okoth et al., 2017). Besides, the results further confirmed that the aptamer was effectively immobilized on the modified electrode, which may be ascribed to the amidation reaction between carboxyl groups of the functionalized MWCNTs and NH_2 groups of the aptamer (Wang et al. 2018a, b). After that, the R_{et} gradually increased with the MCH blocking (curve d, R_{et} = 49.65), because the low conductive proteins hindered interfacial electron transfer. Finally, after being incubated with Tc, the formation

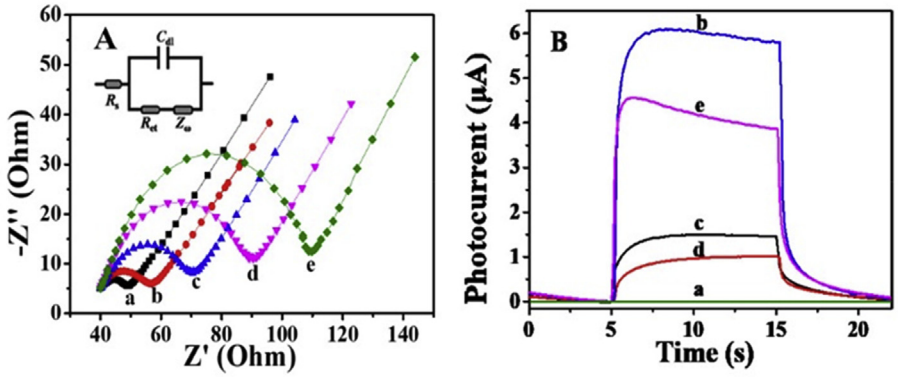

Fig. 4. (A) EIS spectra and (B) Corresponding photocurrent of the modified ITO electrode of the modified ITO electrode: (a) ITO, (b) ITO/MIL-68(In)-NH_2/MWCNT/CdS, (c) ITO/MIL-68(In)-NH_2/MWCNT/CdS/aptamer, (d) ITO/MIL-68(In)-NH_2/MWCNT/CdS/aptamer/MCH and (e) ITO/MIL-68(In)-NH_2/MWCNT/CdS/aptamer/MCH/Tc.

of aptamer-Tc complex blocked the electron transfer between electrode and $[Fe(CN)6]^{3-/4-}$ species (Okoth et al., 2018), leading to significantly increased R_{et} (curve e, R_{et} = 64.64). The values of R_s, Z_ω, C_{dl} and R_{et} are shown in Table S2.

The fabricating process of the PEC aptasensor can also be investigated by photocurrent response. As illustrated in Fig. 4B, the photocurrent of bare ITO electrode was minuscule (curve a). When MIL-68(In)-NH_2/MWCNT/CdS was dropped onto the ITO, the photocurrent exhibited peak value (curve b). Subsequently, the photocurrent response decreased after aptamer anchoring (curve c) and MCH blocking (curve d), the photocurrent intensity gradually decreased due to the increased resistance of the electrode surface, which were consistent with EIS results. However, when aptamer specifically bound with Tc, the Tc molecule was oxidized by photogenerated holes, resulting in an obviously enhanced photocurrent response (curve e). All of the above results prove that the sensor is prepared successfully.

3.4. Optimization of experimental conditions

Fig. S4A explained the photocurrent of ITO/MIL-68(In)-NH_2/MWCNT/CdS electrodes with different CdS ratios. As shown, as the increase of CdS ratios from 20% to 40%, the photocurrent reached maximum, and then gradually decreased when the dose of CdS increased to 60%. These results demonstrate that an appropriate amount of CdS can effectively inhibit the recombination of electrons and holes, but excessive CdS will produce superfluous heterojunction interface, shielding the active sites and inhibiting the separation of electrons and holes. Fig. S4B showed the effect of applied potential on PEC performance. The applied potential varies from +0.2 V to +0.9 V. When the applied potential increases from +0.2 V to +0.5 V, the photocurrent signal gradually increases and reaches a maximum at +0.5 V. But, when the voltage is higher than +0.5 V, an excessively high voltage may cause damage to the electrode surface. Therefore, +0.5 V was selected as the optimal excitation voltage.

The pH of the electrolyte was a key determining factor for the PEC aptasensor. Fig. S4C exhibited the effect of different pH on the photocurrent signal, the photocurrent reaches maximum value when pH = 7.4, which is resembles the physiological pH. This is because that the neutral surroundings could retain the biological activity of protein. PBS (pH = 7.4) was chosen in this work.

The concentration of the aptamer is a critical factor for the performance of PEC aptasensor. As shown in Fig. S4D, with the concentration of the aptamer increasing from 0.5 μmol L^{-1} to 2 μmol L^{-1}, the photocurrent signal gradually declined. However, when the concentration exceeds 1.5 μmol L^{-1}, the photocurrent intensity is almost no longer reduced, reaching a stable level. Therefore, the optimum aptamer concentration for this experiment was 1.5 μmol L^{-1}.

3.5. PEC detect of Tc

Fig. 5A showed the photocurrent intensity of modified electrodes for Tc detection. Under optimal conditions, with the increase of target Tc concentration from 0.1 nmol L^{-1} to 1 μmol L^{-1}, the photocurrent intensity gradually increased. A good linear relationship between the reduction of photocurrent intensity and the logarithm of Tc at different concentrations shown in Fig. 5B. The linear equation was $I = 0.656 \lg c + 2.018$ and the correlation coefficient was 0.992, the LOD was 0.015 nmol L^{-1} (S/N = 3). Compared with other reported methods for Tc detection, our designed PEC aptasensor exhibited an acceptable result (Table S3).

3.6. Selectivity, stability and reproducibility of the aptasensor

To evaluate the selectivity of the proposed aptasensor, several representative antibiotics involving chloramphenicol, ciprofloxacin and diclofenac were selected as interfering substances for the interference test. As displayed in Fig. 5C, under the same experimental conditions, there was no obvious photocurrent change after the addition of a 100 - fold excess of other interfering agents to Tc. When the aptamer is only exposed to interfering substances, all these antibiotics do not exhibit significant responses compared to Tc, it could be attributed to the MCH blocking the non-specific binding of aptamer, resulting the interfering substances cannot be adsorbed to the electrode surface, which proved that the prepared PEC sensor had satisfactory selectivity for Tc detection.

Fig. 5D showed the stability of the designed PEC aptasensor. Switching lights were repeated 20 times in 400s, and the photocurrent responses displayed no remarkable variation during this time, indicating the stable readout of PEC signal. These results indicated that the PEC aptasensor had excellent stability.

For the inspection of reproducibility of the PEC aptasensor, 0.5 nmol L^{-1} Tc was measured with five paralleled electrodes under the same conditions, and the results were shown in Fig. S5. The relative standard deviation (RSD) value was 1.4%, showing the fabricated PEC aptasensor had an acceptable reproducibility.

3.7. Real sample analysis

In order to evaluate the accuracy of the aptasensor in real sample applications, the tap water and lake water were adopted as samples, the recovery of Tc was measured using a standard addition method. Under optimal conditions, 50, 100, 300 nmol L^{-1} of the standard free-Tc were added to a water sample. The results were shown in Table S4, the recovery range was 98.4%–102.1%, and the obtained RSD was 1.0%–2.6%. These results demonstrated that the designed PEC aptasensor could be applied to the water sample detection in environment.

4. Conclusion

To sum up, a label-free Tc-aptasensor has been successfully constructed basing on hierarchical MIL-68(In)-NH_2/MWCNT/CdS composites. The coupling of MWCNTs and MIL-68(In)-NH_2/CdS heterojunction adjusted the electron transport routes and accelerated the charge transfer, which further improved the photoelectric conversion efficiency of PEC electrode, and thus enhanced the PEC aptasensor performance. Profiting from the excellent PEC performance of the well-design sensing platform, a low detection limit of 0.015 nmol L^{-1} as well as a linear range from 0.1 nmol L^{-1} to 1 μmol L^{-1} were obtained for Tc detection. Compared with some representative methods, the PEC aptasensor exhibited a satisfactory result. At the same time, the proposed PEC platform exhibited high selectivity, acceptable sensitivity and stability, which extends a promising application in environmental detection.

CRediT authorship contribution statement

Xue Zhang: Conceptualization, Data curation, Writing - original draft. **Tao Yan:** Conceptualization, Formal analysis. **Tingting Wu:** Methodology, Writing - review & editing. **Yixuan Feng:** Methodology, Writing - review & editing. **Meng Sun:** Formal analysis, Methodology. **Liangguo Yan:** Investigation. **Bin Du:** Funding acquisition, Project administration. **Qin Wei:** Funding acquisition, Project administration.

Acknowledgments

This study was supported by the National Natural Science Foundation of China (21505051, 21575050, 21777056), National Key Scientific Instrument and Equipment Development Project of China (No.21627809), the Key Research and Development Program of Shandong Province (2016GSF117002), the Shandong Provincial Natural Science Foundation (ZR2016BQ12), the Special project of independent innovation and achievements transformation of Shandong

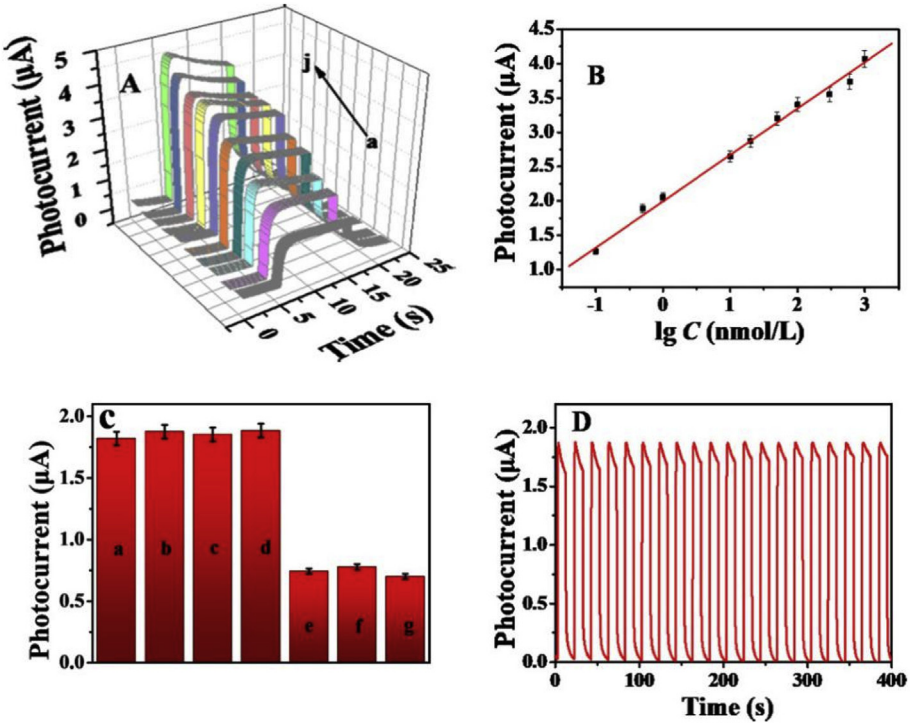

Fig. 5. (A) Photocurrent intensity of modified electrode in the presence of different Tc concentrations (0.1 nmol L^{-1} to 1 μmol L^{-1}); (B) Logarithmic calibration curve determination of various concentrations of Tc; (C) Selectivity of the PEC aptasensor to Tc, (a) Tc, (b) Tc + chloramphenicol, (c) Tc + ciprofloxacin, (d) Tc + diclofenac, (e) chloramphenicol, (f) ciprofloxacin, (g) diclofenac; (D) The stability of the sensor under several switch lights cycles for 400s.

Province (2014ZZCX05101), and QW thanks the Special Foundation for Taishan Scholar Professorship of Shandong Province (No. ts20130937) and UJN.

Appendix A. Supplementary data

Supplementary data to this article can be found online at https://doi.org/10.1016/j.bios.2019.03.062.

References

Alvaro, M., Carbonell, E., Ferrer, B., Llabres i Xamena, F.X., Garcia, H., 2007. Chemistry 13 (18), 5106–5112.
Bagheri, M., Masoomi, M.Y., Morsali, A., 2017. ACS Catal. 7 (10), 6949–6956.
Chen, J., Kong, L., Sun, X., Feng, J., Chen, Z., Fan, D., Wei, Q., 2018. Biosens. Bioelectron. 117, 340–346.
Cheng, C., Amini, A., Zhu, C., Xu, Z., Song, H., Wang, N., 2014. Sci. Rep. 4, 4181.
Choi, K.J., Kim, S.G., Kim, C.W., Kim, S.H., 2007. Chemosphere 66 (6), 977–984.
Dai, H., Zhang, S., Hong, Z., Li, X., Xu, G., Lin, Y., Chen, G., 2014. Anal. Chem. 86 (13), 6418–6424.
Devkota, L., Nguyen, L.T., Vu, T.T., Piro, B., 2018. Electrochim. Acta 270, 535–542.
Dhakshinamoorthy, A., Alvaro, M., Garcia, H., 2010. Chemistry 16 (28), 8530–8536.
Gomes Silva, C., Luz, I., Llabres i Xamena, F.X., Corma, A., Garcia, H., 2010. Chemistry 16 (36), 11133–11138.
Han, Q., Wang, R., Xing, B., Chi, H., Wu, D., Wei, Q., 2018. Biosens. Bioelectron. 106, 7–13.
He, J., Yan, Z., Wang, J., Xie, J., Jiang, L., Shi, Y., Yuan, F., Yu, F., Sun, Y., 2013. Chem. Commun. 49 (60), 6761–6763.
Ke, F., Wang, L.H., Zhu, J.F., 2015. Nano Res 8 (6), 1834–1846.
Leng, F.C., Liu, H., Ding, M.L., Lin, Q.P., Jiang, H.L., 2018. ACS Catal. 8 (5), 4583–4590.
Li, W., Li, D., Zhang, W., Hu, Y., He, Y., Fu, X., 2010. J. Phys. Chem. C 114 (5), 2154–2159.
Li, X.R., Le, Z.Y., Chen, X.L., Li, Z.Q., Wang, W.C., Liu, X.Y., Wu, A., Xu, P.C., Zhang, D.Q., 2018. Appl. Catal. B Environ. 236, 501–508.
Liang, R., Shen, L., Jing, F., Wu, W., Qin, N., Lin, R., Wu, L., 2015. Appl. Catal. B Environ. 162, 245–251.
Liao, T., Kou, L.Z., Du, A.J., Gu, Y.T., Sun, Z.Q., 2018. J. Am. Chem. Soc. 140 (29), 9159–9166.
Liu, H., Chen, L., Ding, J., 2017. Microchim. Acta 184 (10), 4091–4098.
Liu, M., Li, J., 2016. ACS Appl. Mater. Interfaces 8 (3), 2158–2165.
Liu, Y., Gan, X., Zhou, B., Xiong, B., Li, J., Dong, C., Bai, J., Cai, W., 2009. J. Hazard Mater. 171 (1–3), 678–683.
Liu, Y., Yang, H., Yang, S., Hu, Q., Cheng, H., Liu, H., Qiu, Y., 2013. J. Chromatogr. B 917–918, 11–17.
Ma, H., Li, X., Yan, T., Li, Y., Liu, H., Zhang, Y., Wu, D., Du, B., Wei, Q., 2016. ACS Appl. Mater. Interfaces 8 (16), 10121–10127.
Okoth, O.K., Yan, K., Feng, J., Zhang, J.D., 2018. Sens. Actuators B-Chem. 256, 334–341.
Okoth, O.K., Yan, K., Zhang, J.D., 2017. Carbon 120, 194–202.
Pi, Y., Li, X., Xia, Q., Wu, J., Li, Z., Li, Y., Xiao, J., 2017. Nano Res 10 (10), 3543–3556.
Qin, J.S., Du, D.Y., Li, W.L., Zhang, J.P., Li, S.L., Su, Z.M., Wang, X.L., Xu, Q., Shao, K.Z., Lan, Y.Q., 2012. Chem. Sci. 3 (6), 2114.
Sanchez, C., Julián, B., Belleville, P., Popall, M., 2005. J. Mater. Chem. 15 (35–36), 3559.
Song, Z., Ma, Y.L., Li, C.E., Xu, M., 2018. Chem. Eng. 348, 898–907.
Spagnol, V., Sutter, E., Debiemme-Chouvy, C., Cachet, H., Baroux, B., 2009. Electrochim. Acta 54 (4), 1228–1232.
Sun, H., Ahmad, M., Luo, J., Shi, Y., Shen, W., Zhu, J., 2014. Mater. Res. Bull. 49, 319–324.
Swain, G., Sultana, S., Naik, B., Parida, K., 2017. ACS Omega 2 (7), 3745–3753.
Tachikawa, T., Fujitsuka, M., Majima, T., 2007. J. Phys. Chem. C 111 (14), 5259–5275.
Wang, H., Yuan, X.Z., Wu, Y., Zeng, G.M., Chen, X.H., Leng, L.J., Wu, Z.B., Jiang, L.B., Li, H., 2015. J. Hazard Mater. 286, 187–194.
Wang, J., Ma, X., Qu, F., Asiri, A.M., Sun, X., 2017. Inorg. Chem. 56 (3), 1041–1044.
Wang, M.Q., Ye, C., Bao, S.J., Zhang, Y., Yu, Y.N., Xu, M.W., 2016a. Analyst 141 (4), 1279–1285.
Wang, S., Gao, S., Sun, S., Yang, Y., Zhang, Y., Liu, J., Dong, Y., Su, H., Tan, T., 2016b. RSC Adv. 6 (51), 45645–45651.
Wang, Y., Bian, F., Qin, X.F., Wang, Q.Q., 2018a. Microchimica Acta 185 (3), 10.
Wang, Y., Wang, P.P., Wu, Y., Di, J.W., 2018b. Sensor. Actuator. B Chem. 254, 910–915.
Wu, L., Xue, M., Qiu, S.L., Chaplais, G., Simon-Masseron, A., Patarin, J., 2012. Micropor. Mesopor. Mat. 157, 75–81.
Wu, T., Yan, T., Zhang, X., Feng, Y., Wei, D., Sun, M., Du, B., Wei, Q., 2018a. Biosens. Bioelectron. 117, 575–582.
Wu, T., Zhang, Y., Wei, D., Wang, X., Yan, T., Du, B., Wei, Q., 2018b. Sens. Actuators B-Chem. 256, 812–819.
Yang, C., You, X., Cheng, J., Zheng, H., Chen, Y., 2017. Appl. Catal. B Environ. 200, 673–680.
Yu, J.G., Jin, J., Cheng, B., Jaroniec, M., 2014. J. Mater. Chem. 2 (10), 3407–3416.
Yu, W., Zhan, S., Shen, Z., Zhou, Q., 2018. Chem. Eng. J. 345, 462–470.
Zang, Y., Lei, J., Ju, H., 2017. Biosens. Bioelectron. 96, 8–16.
Zhang, Y., Yan, M., Ge, S., Ma, C., Yu, J., Song, X., 2016. J. Mater. Chem. B 4 (29), 4980–4987.
Zhao, W.W., Xu, J.J., Chen, H.Y., 2014. Chem. Rev. 114 (15), 7421–7441.
Zhou, C., Zou, H., Sun, C., Ren, D., Xiong, W., Li, Y., 2018. Anal. Bioanal. Chem. 410 (12), 2981–2989.
Zhu, C., Wei, L., Yuan, P., Xiong, L., Cheng, X., 2016. Instrum. Sci. Technol. 45 (2), 219–231.